Electronic supplement to the paper "A microstructual approach to bedload transport: mean behaviour and fluctuations of particle transport rates"

C. ANCEY AND J. HEYMAN
Environmental Hydraulics Laboratory,
École Polytechnique Fédérale de Lausanne, 1015 Lausanne, Switzerland

(Received December 2013)

The objective of this electronic supplement is to provide further information on the experimental protocol and calculations presented in the body of our paper. The contents are the following:

- Nomenclature, § 1,
- Definition of the local particle transport rate, § 2,
- Decomposition of motion into advection and dispersion, § 3,
- Poisson representation, § 4,
- Steady state solution of the Feller equation, § 5,
- Langevin formulation and calculations of the a moments, § 6,
- Link between the n and a moments, § 7,
- Time correlation functions, § 8,
- Fourier transforms, § 9,
- Experiments 1: velocity probability distribution, § 10,
- Experiments 2: probability distribution of the particle transport rate for a xed bed, § 11,
- Experiments 3: probability distribution of the particle transport rate for a mobile bed, § 12.

1. Nomenclature

Here we provide the list of variables used in the paper, their meaning, physical units, and the reference to the equations or sections, in which they were introduced. In the present document, numbering differs from that used in the paper. Wherever necessary, we make clear whether we refer to an equation in the paper or in this document.

Roman symbols

Variable	Meaning
A	drift function, Eq. (4.15)
$\mathcal{A}$	surface
a, $\boldsymbol{a}$	Poisson rate

Variable	Meaning
a_i	Poisson rate for cell i, Eq. (4.17)
b	Poisson rate, Eq. (4.18)
B	flume width
C	Time correlation function
d	particle diameter
$\mathcal{D}$	diffusivity
d_i	local diffusion rate, Eq. (4.11)
D	diffusion function
D_u	particle diffusivity, Eq. (3.8)
D	deposition rate per unit area in $\mathrm{m\,s^{-1}}$, Eq. (1.3)
E	entrainment rate per unit area in $\mathrm{s^{-1}}$, Eq. (1.3)
f	probability density function in the a-space
Fr	Froude number $\mathrm{Fr} = \bar{v}/\sqrt{gh}$
G	generating function)
g	gravity acceleration $g = 9.81\ \mathrm{m\,s^{-2}}$
g_b	spatial correlation function for b, Eq. (4.19)
g_γ	spatial correlation function for γ, Eq. (4.24)
h	flow depth, Eq. (1.1)
K	kernel function
k	dummy variable
$\boldsymbol{k}$	unit vector
L_z	differential operator
ℓ_c	correlation length, Eq. (4.21)
M_a	differential operator, this document
M_a^*	adjoint differential operator
N	number of particles within the window
N_0	initial number of particles within the window
$\langle N \rangle$	mean number of particles within the window
$\dot{n}$	instantaneous particle flow rate in beads/s, Eq. (2.2)
p	parameter of the negative binomial distribution, Eq. (3.2)
P	probability density function
P_s	probability density function for steady-state processes
Pe	Péclet number $\mathrm{Pe} = \bar{u}_s \Delta x / D_u$, Eq. (4.8)
$\mathcal{Q}$	macroscopic sediment transport rate per unit width in $\mathrm{m^2\,s^{-1}}$, Eq. (6.1)
Q_s	volume particle flow rate in $\mathrm{m^3\,s^{-1}}$
$\bar{q}_s$	mean volume particle sediment rate per unit width in $\mathrm{m^2\,s^{-1}}$
q_s	instances particle sediment rate per unit width in $\mathrm{m^2\,s^{-1}}$, Eq. (2.1)
$\boldsymbol{r}$	position vector
r_p	parameter of the Poisson distribution, Eq. (3.5)
r_{nb}	parameter of the negative binomial distribution, Eq. (3.2)
R	ratio $\mathrm{R} = \ell_c/\Delta x$
Re	flow Reynolds number $\mathrm{Re} = \bar{v}h/\nu_w$
S	wavenumber spectrum, Eq. (4.27)
Sh	Shields number $\mathrm{Fr} = \varrho h \sin\theta / [(\varrho_p - \varrho)d]$
t	time
t_r	relaxation time)
t_c	autocorrelation time
t_a	characteristic time of advection, Eq. (4.8)

Variable	Meaning
t_d	characteristic time of diffusion, Eq. (4.8)
$\mathcal{U}_n$	arithmetic particle velocity for an ensemble of n particles, Eq. (2.1)
$\bar{u}_s$	mean particle velocity in $\mathrm{m\,s^{-1}}$
u_p, $\boldsymbol{u}_p$	particle velocity in $\mathrm{m\,s^{-1}}$
$\bar{v}$	fluid velocity in $\mathrm{m\,s^{-1}}$, Eq. (1.1) and (1.2)
$\mathcal{V}$	control volume
W	Wiener process
W_i	local Wiener process, Eq. (4.17)
x	streamwise coordinate, figure 1
$\boldsymbol{x}$	position vector
y	normal coordinate, figure 1
y_s	elevation of the free surface, figure 1
y_b	elevation of the bed surface, figure 1
z	dummy variable of the generating function
z	space coordinate

Greek and compound symbols

variable	meaning
α	parameter of the Gamma distribution
β	parameter of the Gamma distribution
δ	Kronecker symbol
η	dimensionless groupe $\eta = \Delta x/(\bar{u}_s \Delta t)$
Δt	time increment
Δx	space increment
ϵ	error
γ	particle activity, Eq. (2.1) in m
Γ	gamma function
Γ_o	strength of the initial sediment pulse, § 4.1
κ	difference $\kappa = \sigma - \mu$ in $1\,\mathrm{s^{-1}}$
λ	volumetric entrainment rate per unit area in $\mathrm{m\,s^{-1}}$
λ'	entrainment rate in $1\,\mathrm{s^{-1}}$
μ	collective entrainment rate in $1\,\mathrm{s^{-1}}$
ν	dummy variable
ν_w	kinematic water viscosity in $\mathrm{m^2\,s^{-1}}$
$\boldsymbol{\omega}$	rotation velocity in $\mathrm{rad\,s^{-1}}$
ω	angular frequency in the Fourier transform
ϕ	particle concentration
ϱ	fluid density in $\mathrm{kg\ m^{-3}}$
ϱ_p	particle density in $\mathrm{kg\ m^{-3}}$
σ	deposition rate in $1\,\mathrm{s^{-1}}$
τ_b	bottom shear stress in Pa, Eq. (1.2)
τ	lag time in s
θ	local bed slope, Eq. (1.2)
ϖ_p	particle volume per unit width in $\mathrm{m^2}$
ξ	Gaussian noise increment in $\mathrm{s^{-1/2}}$
ξ_b	space and time Gaussian noise increment in $\mathrm{m^{-1/2}s^{-1/2}}$, Eq. (4.18)

variable	meaning
ζ_b	bed porosity, Eq. (1.3)
ζ	dimensionless group

2. Definition of the local sediment transport rate at the microscopic scale

In this section, we pay special attention to the definition of the sediment transport rate within a probabilistic framework. The physical system under investigation is composed of an array of N_m spherical particles with diameter d. Most of these particles are stationary, forming the granular bed over which the water stream flows, but some of them can be entrained and transported by the flow. The state of the system is described by a state vector $\boldsymbol{S}$ comprising the positions of the centres of mass of the labelled particles $\boldsymbol{x}_k$, their translational velocities $\boldsymbol{u}_{p,k}$ and their rotational velocities $\boldsymbol{\omega}_k$. We also assume that the system has reached a statistically stationary state, i.e. the probability $P(\boldsymbol{S}|\bar{v},h)$ of finding the system in a given configuration $\boldsymbol{S}$ does not depend explicitly on time t. Here, $P(\boldsymbol{S}|\bar{v},h)\mathrm{d}\boldsymbol{x}_1\cdots\mathrm{d}\boldsymbol{x}_{N_m}\mathrm{d}\boldsymbol{u}_1\cdots\mathrm{d}\boldsymbol{u}_{N_m}\mathrm{d}\boldsymbol{\omega}_1\cdots\mathrm{d}\boldsymbol{\omega}_{N_m}$ denotes the probability that the centres of mass are found simultaneously in the volume element $\mathrm{d}\boldsymbol{x}_1$ about the point $\boldsymbol{x}_1$, $\mathrm{d}\boldsymbol{x}_2$ about the point $\boldsymbol{x}_2$, etc, with the respective velocities $(\boldsymbol{u}_1,\boldsymbol{\omega}_1)$, $(\boldsymbol{u}_2,\boldsymbol{\omega}_2)$, etc, given that the water velocity $\bar{v}$ and the flow depth h are known. We also introduce $P_i(\boldsymbol{x},\boldsymbol{u}_p,\boldsymbol{\omega})$, the marginal density probability of finding the particle i at $\boldsymbol{x}$ with translational and rotational velocities $(\boldsymbol{u}_p,\boldsymbol{\omega})$. Similarly, $P_i^x(\boldsymbol{x}) = \int_{\boldsymbol{\omega}}\int_{\boldsymbol{u}_p} P_i(\boldsymbol{x},\boldsymbol{u}_p,\boldsymbol{\omega})\mathrm{d}\boldsymbol{\omega}\mathrm{d}\boldsymbol{u}_p$ denotes the marginal density probability of finding the particle i at $\boldsymbol{x}$. For the sake of simplicity, we do not take into account the conditionality of these probabilities, which depend on the knowledge of $\bar{v}$ and h.

The particle flux Q_s through a surface $\mathcal{A}$ located at a position x is the found by computing the probability that the centre of mass $\boldsymbol{x}_i = (x_i, y_i, z_i)$ of a given particle lies within $x - d/2$ and $x + d/2$ and crosses $\mathcal{A}$ with velocity $\boldsymbol{u} = \boldsymbol{u}_{p,i} + \boldsymbol{\omega}_i \times \boldsymbol{r}$ with $\boldsymbol{r} = \boldsymbol{x}' - \boldsymbol{x}$ the vector from the centre of mass to a point $\boldsymbol{x}'$ of $\mathcal{A}$, then summing up over the state vector (see figure 1) to give

$$Q_s = \sum_{i=1}^{N_m} \int_{x_i=x-a}^{x+a} \mathrm{d}x \int_{y,z} \mathrm{d}y\mathrm{d}z P_i^x(\boldsymbol{x}) \int_{\boldsymbol{x}'\in\mathcal{A}} \mathrm{d}|\boldsymbol{x}'| \int_{\boldsymbol{\omega}}\int_{\boldsymbol{u}_p} P_i(\boldsymbol{u}_p,\boldsymbol{\omega}|\boldsymbol{x};\bar{v},h)(\boldsymbol{u}\cdot\boldsymbol{k})\mathrm{d}\boldsymbol{\omega}\mathrm{d}\boldsymbol{u}_p \tag{2.1}$$

with $\boldsymbol{k}$ the normal to the surface. This definition is prohibitively complex and of little use if we would like to implement it for practical purposes. We use the following assumptions to simplify the problem. First, we assume that we can replace the ensemble average by a volume average over a control volume $\mathcal{V}$ of length Δx, which is arbitrary for the moment, and centred around x. The flow depth varies sufficiently slowly over Δx to be viewed as constant.

Second, as we are mainly interested in a two-dimensional problem, we ignore what happens in the z-direction and consider a particle transport rate per unit width q_s. In the following, any volume is to be understood as a volume per unit width.

Third, we consider that the particle velocities $(\boldsymbol{u}_p,\boldsymbol{\omega})$ depend on the downward projected position x as they are likely to depend on the fluid velocity $\bar{v}$ and depth h, so that we can relax the conditional dependence on the particle position $\boldsymbol{x}$ in P_i : $P_i(\boldsymbol{u}_p,\boldsymbol{\omega}|\boldsymbol{x};\bar{v},h) = P_i(\boldsymbol{u}_p|\bar{v},h)$. Because the volume integration of the rotational velocity field $\boldsymbol{\omega}_i \times \boldsymbol{r}$ is zero, the contribution of the rotational velocity to the velocity flux is zero for all particles entirely contained in the control volume $\mathcal{V}$ (but not, strictly speaking, for particles whose volume lies partially outside $\mathcal{V}$). This implies that

$$\int_{\boldsymbol{\omega}}\int_{\boldsymbol{u}_p} P_i(\boldsymbol{u}_p,\boldsymbol{\omega}|\boldsymbol{x};\bar{v},h)(\boldsymbol{u}\cdot\boldsymbol{k})\mathrm{d}\boldsymbol{\omega}\mathrm{d}\boldsymbol{u}_p \approx \bar{u}_s(\mathcal{V};\bar{v},h) = \frac{1}{\mathcal{V}}\left(\boldsymbol{k}\cdot\int_{\Delta x}\boldsymbol{u}_p\mathrm{d}\mathcal{V}\right), \tag{2.2}$$

$\bar{u}_s(\mathcal{V};\bar{v},h)$ denotes the mean particle velocity inside the control volume $\mathcal{V}$.

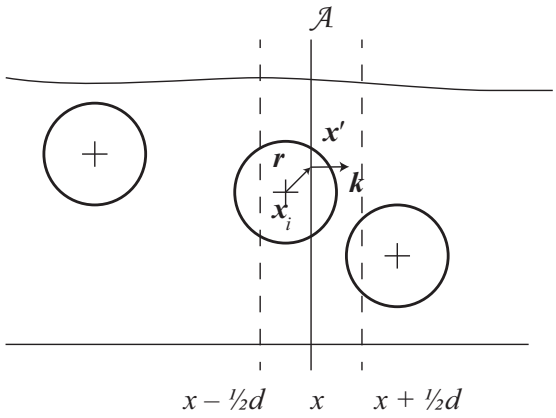

FIGURE 1. Schematic showing the integration of the particle flux.

Fourth, as a first approximation, we assume that the particles are uniformly distributed along the x-direction within $\mathcal{V}$ so that

$$\sum_{i=1}^{N_m} \int_{x_i=x-a}^{x+a} \mathrm{d}x \int_{y,z} \mathrm{d}y\mathrm{d}z P_i^x(\boldsymbol{x}) \int_{\boldsymbol{x}'\in\mathcal{A}} \mathrm{d}|\boldsymbol{x}'| \approx \frac{\mathcal{V}_p}{\mathcal{V}}\mathcal{A} = \phi\mathcal{A}, \tag{2.3}$$

in which $\mathcal{V}_p$ denotes the volume occupied by the particles and $\phi(x,t;\mathcal{V}) = \mathcal{V}_p/\mathcal{V}$ is the (volume) particle concentration within $\mathcal{V}$. If we refer to the number of moving particles in $\mathcal{V}$ as N and to the volume particle (per unit width) as ϖ_p, we can also express $\phi\mathcal{A}$ as $N\varpi_p/\Delta x$.

These assumptions lead us to define the sediment transport rate per unit width (within $\mathcal{V}$) at the microscopic scale as

$$q_s(x,t;\mathcal{V};\bar{v},h) = \phi(x,t;\mathcal{V})h(x,t)\bar{u}_s(\mathcal{V};\bar{v},h), \tag{2.4}$$

or equally, we can define the sediment transport rate as the time variation in the number of moving particles

$$\dot{n} = \frac{N}{\Delta x}\bar{u}_s(\mathcal{V};\bar{v},h). \tag{2.5}$$

In the body of the paper, we have followed Furbish *et al.* (2012) and used the particle activity $\gamma(x,t) = \phi(x,t;\mathcal{V})h(x,t) = N\varpi_p/\Delta x$ rather than the particle concentration.

A word of caution concerns the equivalence between the discrete and continuous variables N and $\gamma(x,t)$. Essentially, when using N, we count the number of particles whose centres of mass are included in the control volume $\mathcal{V}$, whereas $\gamma(x,t)$ represents the volume of the particles inside $\mathcal{V}$. Near the boundaries of $\mathcal{V}$, particles can lie partially outside the volume and therefore, there is a small error induced by the consideration of a strict equivalence between the two variables. To evaluate this error, let us consider three adjacent cells of length Δx. The number of particles in each cell is N_k, with $k = i-1, i$, and $i+1$. We assume that the particles are uniformly distributed within each cell i so that the probability of finding the centre of mass of a particle at abscissa x is given by the uniform distribution $p_i(x) = N_i/\Delta x$. All of the particles for which the distance r

between the centre of mass and the cell boundary is lower than $d/2$ cross this boundary and part of their volume is to be excluded from the total particle volume in the cell. For a particle that is a distance r away from the boundary, the excluded volume is

$$V(r) = \pi \left(\frac{d}{2}\right)^3 \int_\theta^{\pi/2} \sin^3\psi \mathrm{d}\psi = \pi \left(\frac{d}{2}\right)^3 \left(2\frac{r}{d} - \frac{2}{3}\left(\frac{r}{d}\right)^3\right) \text{ with } \cos\theta = 2\frac{r}{d}. \quad (2.6)$$

The total excluded volume from cell i is then

$$V_i^{excl.} = \int_0^{d/2} p_i(r)V(r)\mathrm{d}r = \frac{5}{192}\frac{\pi d^4}{\Delta x}N_i \quad (2.7)$$

The adjacent cells $i-1$ and $i+1$ also have protruding particles and therefore, the volume balance is

$$V_i^{bal.} = \int_0^{d/2} p_i(r)V(r)\mathrm{d}r = \frac{5}{192}\frac{\pi d^4}{\Delta x}(2N_i - N_{i+1} - N_{i-1}), \quad (2.8)$$

leading to a relative error

$$\epsilon = \frac{V_i^{bal.}}{N\frac{4}{3}\pi\left(\frac{d}{2}\right)^3} = \frac{5}{32}\frac{d}{\Delta x}\frac{2N_i - N_{i+1} - N_{i-1}}{N_i}, \quad (2.9)$$

which is $o(d/\Delta x)$. Note that in the limit of $\Delta x \to 0$, we can interpret the last term on the right-hand side of (2.9) as a second-order finite difference and thus,

$$\epsilon = -\frac{5}{32}\frac{d\Delta x}{\gamma}\frac{\partial^2\gamma}{\partial x^2}, \quad (2.10)$$

showing that $\epsilon \to 0$ provided that γ is locally nonzero.

3. Advection and dispersion of a particle cloud

3.1. *Calculation of the diffusion coefficient $\mathcal{D}$*

The objective of this appendix is to show that (i) the displacement processes occurring in a particle cloud during a time increment Δt can be broken down into advection and isotropic dispersion under certain conditions, (ii) we can calculate the coefficient of diffusion from the various parameters, in particular the particle diffusivity D_u. Let us consider that at time t, there is a cloud of N particles uniformly occupying the control volume $\mathcal{V}$ of length Δx, as shown by figure 2. The probability of finding the particle at $x \in [0, \Delta x]$ is then the uniform distribution $f_x(x) = N/\Delta x$ if $x \in [0, \Delta x]$, and $f_x(x) = 0$ for $x \notin [0, \Delta x]$.

Each particle moves at a velocity U, whose probability distribution is given by the truncated Gaussian distribution (3.11) of the paper

$$f_u(u) = \sqrt{\frac{2}{\pi}}\frac{\zeta}{\bar{u}_s}\frac{1}{1+\mathrm{erf}(\zeta/\sqrt{2})}\exp\left(-\frac{\zeta^2}{2}\left(\frac{u}{\bar{u}_s} - 1\right)^2\right) \text{ with } \zeta = \bar{u}_s\sqrt{\frac{t_r}{D_u}}. \quad (3.1)$$

At time $t + \Delta t$, a particle initially at x will have moved at

$$x' = x + u\Delta t, \quad (3.2)$$

or in a dimensionless form

$$\tilde{x}' = \tilde{x} + \eta^{-1}\tilde{u} \text{ with } \eta = \frac{\Delta x}{\bar{u}_s \Delta t}, \quad (3.3)$$

where the variables have been scaled as follows: $\tilde{x} = x/\Delta x$ and $\tilde{u} = u/\bar{u}_s$. The probability

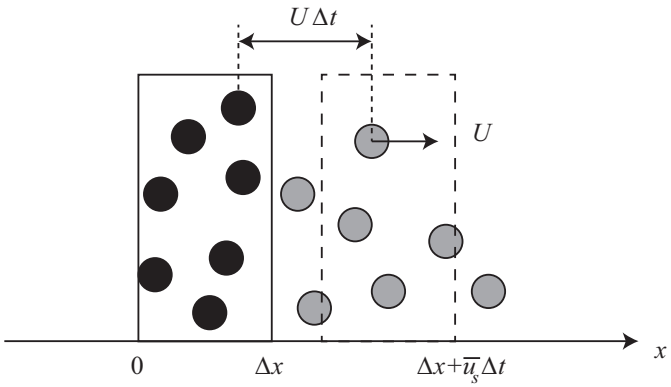

FIGURE 2. At time t, the volume $[0, \Delta x]$ contains N particles (in black). We are interested in calculating the displacement of the particles at time $t+\Delta t$ knowing that the velocity probability distribution of the particles is $f_u(u)$.

distribution of $\tilde{x}'$ is related to the scaled convolution of the probability distributions of x and u:

$$\begin{aligned} f_{\tilde{x}'}(\tilde{x}') &= G_u(\zeta,\eta) N \int_0^{\min(\tilde{x}',1)} F_u(\tilde{x}'-\tilde{x},\zeta,\eta)\mathrm{d}\tilde{x}, \\ &= N \frac{\mathrm{erf}\left(\dfrac{\zeta}{\sqrt{2}}(1-\eta\max(0,\tilde{x}'-1))\right) - \mathrm{erf}\left(\dfrac{\zeta}{\sqrt{2}}(1-\eta\tilde{x}')\right)}{1+\mathrm{erf}\left(\dfrac{\zeta}{\sqrt{2}}\right)}, \end{aligned} \tag{3.4}$$

where we have introduced the following functions (stemming from the velocity distribution made dimensionless):

$$G_u(\zeta,\eta) = \sqrt{\frac{2}{\pi}} \frac{\eta\zeta}{1+\mathrm{erf}(\zeta/\sqrt{2})} \text{ and } F_u(\nu,\zeta,\eta) = \exp\left(-\frac{\zeta^2}{2}(\eta\nu-1)^2\right). \tag{3.5}$$

Theoretically, we expect that the cloud has been advected by the water stream at the mean velocity $\bar{u}_s$. If all of the particles were advected at this velocity, then the cloud initially occupying $[0,1]$ (in the dimensionless space) would then span over $[\eta^{-1}, 1+\eta^{-1}]$ at the later time $t+\Delta t$. However, as the particles' velocity fluctuates, some of the particles will lie outside this interval. Some of them will lag behind

$$N_{left} = \int_0^{1/\eta} f_{\tilde{x}'}(\tilde{x}')\mathrm{d}\tilde{x}' = N\frac{1}{\eta\zeta}\sqrt{\frac{2}{\pi}}\frac{1-\exp[-\zeta^2/2]}{1+\mathrm{erf}(\zeta/\sqrt{2})} \tag{3.6}$$

while others will be ahead of this interval:

$$N_{right} = \int_{1+1/\eta}^{\infty} f_{\tilde{x}'}(\tilde{x}')\mathrm{d}\tilde{x}' = \frac{N}{\eta\zeta}\sqrt{\frac{2}{\pi}}\frac{1-\exp[-\eta^2\zeta^2/2]}{1+\mathrm{erf}(\zeta/\sqrt{2})} + N\frac{1-\mathrm{erf}(\zeta\eta/\sqrt{2})}{1+\mathrm{erf}(\zeta/\sqrt{2})}. \tag{3.7}$$

For $\zeta > 2$, due to the fast decay in the ζ contributions, the two relative outflow numbers are nearly identical. For $\zeta \sim 1$, these numbers differ significantly, by approximately a factor of 2, as shown by figure 3. This shows that when $\zeta > 2$, the displacement of the cloud can be split into two parts: a translation due to advection (displacement at the mean velocity $\bar{u}_s$) and scattering with a scaled coefficient of diffusion. Figure 4 plots the probability density function $f_{\tilde{x}'}(\tilde{x}')$ for three values of ζ (and for $\eta = 1$): for low ζ values (here $\zeta = 1$), the distribution is markedly asymmetric while at larger ζ values

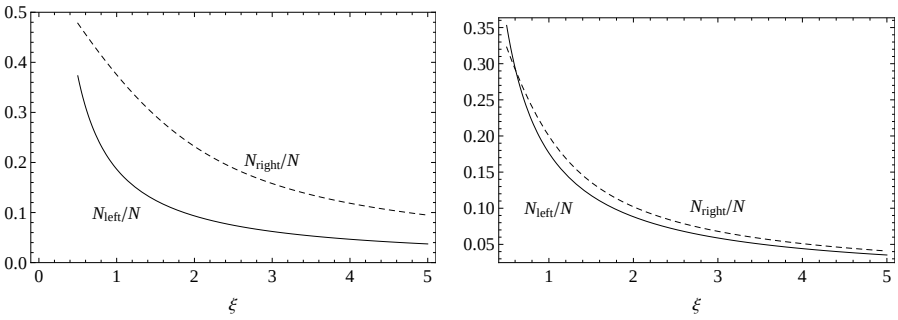

FIGURE 3. Variation in N_{left}/N and N_{right}/N as a function of η for $\zeta = 1$ (on the left) and $\zeta = 2$ (on the right). For $\zeta \geqslant 3$, the curves N_{left}/N and N_{right}/N collapse.

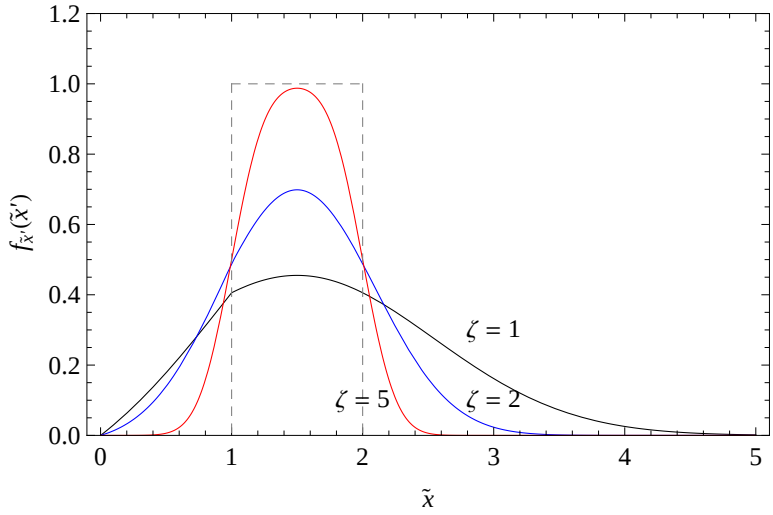

FIGURE 4. Probability density function of the position $\tilde{x}'$ for $\eta = 1$ and three different values of ζ: $\zeta = 1$ (black online), $\zeta = 2$ (blue online), and $\zeta = 5$ (red online). The dashed line represents the advection of the initial control volume (displacement by η^{-1} in the dimensionless space).

(here $\zeta = 5$), the shape of the distribution approaches that of a normal distribution. This shows that for $\zeta < 2$, particle velocity fluctuations give rise to anisotropic scattering, which contrasts to our simple jump process (4.11) in the paper.

To calculate the diffusion coefficient $\mathcal{D}$, let us draw an analogy with the following initial boundary-value problem, in which N particles contained in a narrow box $[0, \Delta x]$ are released at $t = 0$. The particle concentration $\phi(x)$ follows the diffusion equation

$$\frac{\partial \phi}{\partial t} = \mathcal{D}\frac{\partial^2 \phi}{\partial x^2}, \tag{3.8}$$

subject to $\phi(x, 0) = N/\Delta x$ for $0 \leqslant x \leqslant \Delta x$ and $\phi(x, 0) = 0$ for $x \notin [0, \Delta x]$, $\phi(\pm\infty, t) = 0$, and $\int_x \phi(x, t)\mathrm{d}x = N$. The solution is

$$\phi(x, t) = \frac{1}{2}\mathrm{erf}\left(\frac{x}{\sqrt{4\mathcal{D}t}}\right) - \frac{1}{2}\mathrm{erf}\left(\frac{x - \Delta x}{\sqrt{4\mathcal{D}t}}\right). \tag{3.9}$$

In a dimensionless form, the variance at a time Δt after release is found to be

$$\operatorname{var}\phi = N\left(\frac{1}{12} + 2\frac{\mathcal{D}}{\bar{u}_s^2\Delta t}\eta^{-2}\right). \tag{3.10}$$

As the initial and boundary values are the same for the two problems, we expect that the moments of the distributions (3.9) and (3.4) match at early times, which should give a way of estimating $\mathcal{D}$. From (3.4), we can compute the variance of the displacement

$$\operatorname{var}\tilde{x}' = N\left(\frac{1}{12} + A(\zeta)\eta^{-2}\right), \tag{3.11}$$

$$A(\zeta) = \frac{\pi + \pi(B^2(\zeta)-1) - \sqrt{2\pi}\zeta B(\zeta)\mathrm{e}^{-\zeta^2/2} - 2\mathrm{e}^{-\zeta^2}}{\pi\zeta^2 B^2(\zeta)} = \frac{1}{\zeta^2} + O(\zeta^{-3}), \tag{3.12}$$

where we have used

$$B(\zeta) = 1 + \operatorname{erf}(\zeta/\sqrt{2}).$$

As the probability of finding a particle at x' can also be interpreted as the concentration ϕ, we can compare the variances (3.10) and (3.9) and deduce an expression for the diffusion coefficient $\mathcal{D}$

$$\mathcal{D} = \frac{1}{2}A(\zeta)\bar{u}_s^2\Delta t \approx \frac{1}{2}\frac{\bar{u}_s^2\Delta t}{\zeta^2} = \frac{1}{2}\frac{\Delta t}{t_r}D_u. \tag{3.13}$$

This shows that if we select the time step Δt properly ($\Delta t = 2t_r$), the two coefficients of diffusion D_u and $\mathcal{D}$ are equal.

3.2. *Probability of a long displacement*

By assuming that diffusion can be treated as a local jump process, we must ensure that some particles are unlikely to travel long distances (super-diffusion), e.g., one particule starting from cell i and arriving at cell $i+k$ with $k > 1$. With the velocity probability distribution (3.1), we can also compute the probability that the displacement of the particles during the time Δt exceeds the length Δx of a control volume $\mathcal{V}$

$$\begin{aligned}\operatorname{Prob}(U > \Delta x/\Delta t) &= \frac{\operatorname{erfc}(\zeta\eta/\sqrt{2})}{1+\operatorname{erf}(\zeta)} \\ &= \mathrm{e}^{-\zeta^2\eta^2}\left(\frac{1}{1+\operatorname{erf}(\zeta)}\frac{1}{\zeta\eta} + O\left(\frac{1}{\zeta^2\eta^2}\right)\right).\end{aligned} \tag{3.14}$$

This excess probability decreases very quickly with $\zeta\eta$. Typically, with $\zeta\eta = 5$, this probability is order 10^{-10}. In practice, this means that most particles will move over a length that is much smaller than the volume length Δx. The probability of a particle jumping from i to $i+2$ or further is vanishingly small.

4. Poisson representation

4.1. *Definition*

Following Gardiner (1983), we assume that we can expand $P(n,t)$ as a superposition of Poisson distributions

$$P(n,t) = \int_a \frac{e^{-a}a^n}{n!}f(a)\mathrm{d}a, \tag{4.1}$$

where the integration is made over a domain to be specified and $f(a)$ is a positive real-valued function. Within the framework of distribution theory, this representation always

exists since if we introduce the distribution

$$f(a;m) = \mathrm{e}^a \left(-\frac{\partial}{\partial a}\right)^m \delta(a)$$

we can check that this is a probability distribution function by integrating by parts

$$\int_a f(a;m)\mathrm{d}a = \int_a \mathrm{e}^a \left(-\frac{\partial}{\partial a}\right)^m \delta(a)\mathrm{d}a = (-1)^{2m}\int_a \mathrm{e}^a\delta(a)\mathrm{d}a = \mathrm{e}^0 = 1$$

as $\partial_a\delta = -\delta$ and for any distribution T and function ϕ, we have $\int T'\phi\mathrm{d}a = -\int T\phi'\mathrm{d}a$. Moreover

$$\begin{aligned}\int_a f(a;m)\frac{e^{-a}a^n}{n!}\mathrm{d}a &= \int_a \frac{a^n}{n!}\left(-\frac{\partial}{\partial a}\right)^m \delta(a)\mathrm{d}a = (-1)^m\frac{m!}{n!}\int_a a^{n-m}\delta(a)\mathrm{d}a,\\ &= a^{n-m}|_{a=0},\\ &= \delta(m-n).\end{aligned}$$

Since the δ function has a representation in the a-space, any probability distribution can formally be represented using the Poisson distribution (4.1).

4.2. *Generating function*

The generating function (3.12) of the paper is equivalent to

$$G(z,t) = \sum_{n=0}^{\infty} z^n \int_a \frac{e^{-a}a^n}{n!} f(a)\mathrm{d}a = \int_a \exp[a(z-1)]f(a,t)\mathrm{d}a, \tag{4.2}$$

which can also be put in functional form

$$G(z,t) = \{K, f\}, \tag{4.3}$$

where the braces and K represent the inner product and the Laplace kernel, respectively

$$\{f,g\} = \int_a f(a)g(a)\mathrm{d}a \text{ and } K(z,a) = \exp[a(z-1)] \tag{4.4}$$

for any functions f and g. We introduce the linear operator (acting on z)

$$L_z[G] = \lambda'(z-1)G + (z-1)(\mu z - \sigma)\frac{\partial}{\partial z}G. \tag{4.5}$$

We are looking an operator M_a acting on a such that

$$L_z[G] = \{L_z[K], f\} = \{M_a[K], f\} \tag{4.6}$$

As we have

$$\begin{aligned}L_z[K] &= \left(\lambda'(z-1) + (z-1)(\mu z-\sigma)\frac{\partial}{\partial z}\right)K, \qquad (4.7)\\ &= \left(\lambda'(z-1) + a(z-1)(\mu z-\sigma)\right)K,\\ &= \left((\lambda' + a(\mu-\sigma))(z-1) + a\mu(z-1)^2\right)K,\\ &= \left((\lambda' + a(\mu-\sigma))\frac{\partial}{\partial a} + a\mu\frac{\partial^2}{\partial a^2}\right)K,\end{aligned}$$

we are then led to define

$$M_a = (\lambda' + a(\mu-\sigma))\frac{\partial}{\partial a} + a\mu\frac{\partial^2}{\partial a^2} \tag{4.8}$$

The adjoint M_a^* of M_a satisfies the relation

$$\{M_a[K], f\} = \{K, M_a^*[f]\} \tag{4.9}$$

Let us integrate by parts

$$\begin{aligned}
\{M_a[K], f\} &= \int_a M_a[K] f(a) \mathrm{d}a, && (4.10)\\
&= \left([K(\lambda' + a(\mu - \sigma))f] - \int_a K \frac{\partial}{\partial a}[(\lambda' + a(\mu - \sigma))f] \mathrm{d}a \right) + && (4.11)\\
&\quad \mu \left(\left[af \frac{\partial K}{\partial a} \right] - \int_a \frac{\partial K}{\partial a} \frac{\partial af}{\partial a} \mathrm{d}a \right), \\
&= \left[K(\lambda' + a(\mu - \sigma))f + \mu af \frac{\partial K}{\partial a} \right] - \int_a K \frac{\partial}{\partial a}[(\lambda' + a(\mu - \sigma))f] \mathrm{d}a - \\
&\quad \mu \left(\left[K \frac{\partial af}{\partial a} \right] - \int_a K \frac{\partial^2 af}{\partial a^2} \mathrm{d}a \right), \\
&= \left[K(\lambda' + a(\mu - \sigma))f + \mu af \frac{\partial K}{\partial a} - \mu K \frac{\partial af}{\partial a} \right] + \\
&\quad \int_a K \left(\mu \frac{\partial^2 af}{\partial a^2} - \frac{\partial}{\partial a}[(\lambda' + a(\mu - \sigma))f] \right) \mathrm{d}a.
\end{aligned}$$

The domain of integration is chosen so that the terms within the square brackets cancel out and if so, we can define the adjoint operator

$$M_a^*[f] = \mu \frac{\partial^2 af}{\partial a^2} - \frac{\partial}{\partial a}[(\lambda' + a(\mu - \sigma))f]. \tag{4.12}$$

To summarize the different steps, we have transformed the initial differential problem

$$\frac{\partial G}{\partial t} = L_z[G] \text{ with } G(z,t) = \{K(z,a), f(a,t)\},$$

into

$$\begin{aligned}
\left\{ K, \frac{\partial f}{\partial t} \right\} &= \{L_z[K], f\} && (4.13)\\
&= \{K, M_a^*[f]\},
\end{aligned}$$

The governing equation for f is then

$$\frac{\partial f}{\partial t} = \mu \frac{\partial^2 af}{\partial a^2} - \frac{\partial}{\partial a}[(\lambda' + a(\mu - \sigma))f]. \tag{4.14}$$

The solution is a density probability function (noncentral chi-square distribution) is found; see Cox *et al.* (1985) for the details. Equation is singular at $a = 0$ (transformation from a parabolic to a hyperbolic problem). The solutions to (4.2) have been studied by Feller (1951) and Sacerdote (1990). Feller (1951) showed that the case $\lambda' < \mu$, the problem is nearly regular and solutions with different boundary conditions can be determined. For $\mu < \lambda'$, there exists a positivity and norm preserving solution of the initial value problem such that both it and its flux vanish at $x = 0$. This means that $x = 0$ acts both as absorbing and reflecting barrier. If the former condition is met ($\lambda' < \mu$), f tends to infinity when $a \to 0$, which means that $a = 0$ corresponds to the highest probabilities (mode of f), but is never reached. In the latter case, $f(a,t) = 0$, the mode of f is somewhere within $(0, \infty)$.

5. Steady state solution of the Feller equation

Under steady state conditions, (4.2) can be integrated twice:

$$\mu \frac{\partial a f}{\partial a} = (\lambda' + a(\mu - \sigma))f + c_1 \tag{5.1}$$

and taking $c_1 = 0$ ($f \to 0$ and $\partial_a(af) \to 0$ when $a \to \infty$), then

$$f(a) = \frac{a^{\lambda'/\mu - 1} \exp[-(\sigma - \mu)a/\mu]}{c_2} \tag{5.2}$$

with c_2 a constant of integration. This can be interpreted as the gamma distribution $\mathrm{Ga}(\alpha, \beta)$ with parameters $\alpha = \lambda'/\mu > 0$ and $\beta = \mu/(\sigma - \mu) > 0$:

$$\mathrm{Ga}(x; \alpha, \beta) = \frac{x^{\alpha - 1} \exp[-x/\beta]}{\Gamma[\alpha]\beta^{\alpha}}$$

This gives the constant of integration : $c_2 = \Gamma[\alpha]\beta^{\alpha}$. We then deduce that

$$P_s(n) = \int_a \frac{e^{-a}a^n}{n!} \mathrm{Ga}(a; \alpha, \beta)\mathrm{d}a = \mathrm{NegBin}(n, r, p) = \frac{\Gamma[r + n]}{\Gamma[r]} p^r (1 - p)^n, \tag{5.3}$$

with $r = \alpha = \lambda'/\mu$ and $p = 1/(1 + \beta) = 1 - \mu/\sigma$. We retrieve the results given above.

6. Langevin formulation and calculations of the a moments

As (4.2) takes the form of a Fokker-Planck equation with the following drift and diffusion functions $A = \lambda' + a(\mu - \sigma)$ and $D = 2\mu a$, we can also interpret the process in terms of a Langevin equation for a

$$\mathrm{d}a = A\mathrm{d}t + \sqrt{D}\mathrm{d}W(t) = (\lambda' + a(\mu - \sigma))\mathrm{d}t + \sqrt{2\mu a}\mathrm{d}W(t), \tag{6.1}$$

with $W(t)$ a Wiener process. Note the amplitude of the noise term. In the absence of collective entrainment ($\mu = 0$ then $D = 0$), the process is purely deterministic and we have

$$\frac{\mathrm{d}a}{\mathrm{d}t} = \lambda' - a(\sigma - \mu) \Rightarrow a(t) = \frac{\lambda'}{\sigma - \mu} + a_0 \exp[-(\sigma - \mu)t].$$

When collective entrainment occurs ($\mu > 0$), the process is random, with a multiplicative noise term. Note that (6.1) has also been studied in economics (Cox *et al.* 1985) to model short-term interest rates and in soil physics to model nitrous oxide emission (Pedersen 2000). In that case, the solution to (6.1) subject to $a(0) = a_0$ is

$$a(t) = a_\infty + (a_0 - a_\infty)\exp[-\kappa t] + \sqrt{2\mu}\exp[-\kappa t]\int_0^t \exp[\kappa t']\sqrt{a(t')}\mathrm{d}W(t'), \tag{6.2}$$

with $a_\infty = \lambda'/(\sigma - \mu)$ the steady-state solution $\kappa = \sigma - \mu$. We then deduce the expectation

$$\langle a(t)\rangle = a_\infty + (a_0 - a_\infty)\exp[-\kappa t]. \tag{6.3}$$

Using the Itô formula, we deduce that a^2 satisfies

$$\mathrm{d}a^2 = 2\left(\mu a + (\lambda' - a(\sigma - \mu))a\right)\mathrm{d}t + 2a\sqrt{2\mu a}\mathrm{d}W(t),$$

then the second-order moment $\langle a^2(t)\rangle$ is given by

$$\frac{\mathrm{d}}{\mathrm{d}t}\langle a^2\rangle = 2(\mu + \lambda')\langle a\rangle - 2(\sigma - \mu)\langle a^2\rangle.$$

After integration and a few algebraic manipulations, we find that the variance is

$$\operatorname{var} a(t) = 2\frac{\mu}{\kappa} a_0 \exp[-2\kappa t](\exp[\kappa t]-1) + \frac{\mu}{\kappa} a_\infty \exp[-2\kappa t](\exp[\kappa t]-1)^2 \tag{6.4}$$

Note that this result can be obtained directly from the solution (6.2) using the fact that a is a non-anticipating function

$$\begin{aligned}
\operatorname{var} a = \langle (a(t)-\langle a\rangle)^2\rangle &= \left\langle 2\mu \exp[-2\kappa t]\left(\int_0^t \exp[\kappa t']\sqrt{a(t')}\mathrm{d}W(t')\right)^2\right\rangle, \qquad (6.5)\\
&= 2\mu\exp[-2\kappa t]\left\langle \left(\int_0^t \exp[\kappa t']\sqrt{a(t')}\mathrm{d}W(t')\right)^2\right\rangle,\\
&= 2\mu\exp[-2\kappa t]\int_0^t \langle \exp[2\kappa t']a(t')\rangle \,\mathrm{d}t',\\
&= 2\mu\exp[-2\kappa t]\int_0^t \exp[2\kappa t']\,\langle a(t')\rangle \,\mathrm{d}t',\\
&= 2\mu\exp[-2\kappa t]\int_0^t \exp[2\kappa t'](a_\infty + (a_0-a_\infty)\exp[-\kappa t'])\mathrm{d}t',\\
&= 2\frac{\mu}{\kappa} a_0 \exp[-2\kappa t](\exp[\kappa t]-1) + \frac{\mu}{\kappa} a_\infty \exp[-2\kappa t](\exp[\kappa t]-1)^2.
\end{aligned}$$

The covariance for $t > s$ is

$$\begin{aligned}
\operatorname{cov}((a(s),a(t)) &= \langle (a(s)-\langle a\rangle)(a(t)-\langle a\rangle)\rangle, \qquad (6.6)\\
&= \left\langle 2\mu\exp[-\kappa(t+s)]\int_0^{\min(s,t)} \langle \exp[2\kappa t']a(t')\right\rangle \mathrm{d}t',\\
&= 2\frac{\mu}{\kappa} a_0 \exp[-\kappa(s+t)](\exp(\kappa s)-1) + \frac{\mu}{\kappa} a_\infty \exp[-\kappa(t+s)](\exp(\kappa s)-1)^2,\\
&= \exp[-\kappa(t-s)]\operatorname{var} a(s),
\end{aligned}$$

which shows that the autocorrelation is

$$\rho(\tau) = \frac{\operatorname{cov}((a(s),a(s+\tau))}{\operatorname{var} a(s)} = \mathrm{e}^{-\kappa\tau}. \tag{6.7}$$

7. Link between the n and a moments

The Poisson representation enjoys a very useful property, which turns out to be very practical as there is no easy way to retrieve $P(n,t)$ from $f(a,t)$. The factorial moments of n are equal to the moments of a

$$\begin{aligned}
\langle n(n-1)(n-2)\ldots(n-p+1)\rangle &= \int_a \sum_{n=0}^{\infty} n(n-1)(n-2)(n-p+1)\frac{e^{-a}a^n}{n!} f(a,t) \qquad (7.1)\\
&= \int_a a^p f(a,t),\\
&= \langle a^p\rangle
\end{aligned}$$

We then have

$$\langle n\rangle = \langle a\rangle \tag{7.2}$$

$$\langle n^2\rangle = \langle a^2\rangle + \langle a\rangle. \tag{7.3}$$

These relationships hold true when taken at the same time t. We can also define conditional averages. For instance, given the initial conditions $a(s) = a'$ and $n(s) = n'$, we define the mean value of a and n at time t as

$$\langle a|(a',s)\rangle = \int_a a f(a,t|a',s)\mathrm{d}a \text{ and } \langle n|(n',s)\rangle = \sum_n nP(n,t|n',s).$$

There is a connection between the initial conditions $a(s) = a'$ and $n(s) = n'$ in the n- and a-spaces. Let us consider the probability distribution

$$f(a,s|a',s) = \mathrm{prob}[a(s) = a'] = \delta(a - a').$$

It is associated with a distribution in the n-space

$$P(n,s|a',s) = \int_a \frac{e^{-a}a^n}{n!} f(a,s|a',s)\mathrm{d}a = \int_a \frac{e^{-a}a^n}{n!}\delta(a-a')\mathrm{d}a = \frac{e^{-a'}a'^n}{n!}. \tag{7.4}$$

At later times, the probability $P(n,t|a',s)$ evolves. It can be determined by summing over all the possible initial conditions $n(s) = n'$ in the n-space

$$P(n,t|a',s) = \sum_{n'} P(n,t|n',s)P(n',s|a',s)$$

This relation makes it possible to link the conditional averages in the n- and a-spaces

$$\begin{aligned}\langle a|(a',s)\rangle &= \int_a a f(a,t|a',s)\mathrm{d}a = \langle n|(a',s)\rangle = \sum_n nP(n,t|a',s) \\ &= \sum_n n \sum_{n'} P(n,t|n',s)P(n',s|a',s), \\ &= \sum_{n,n'} nP(n,t|n',s)\frac{e^{-a'}a'^{n'}}{n'!}, \\ &= \sum_{n'} \langle n|(n',s)\rangle \frac{e^{-a'}a'^{n'}}{n'!}.\end{aligned} \tag{7.5}$$

8. Time correlation functions

The relationship between the covariances $\langle n(t)n(s)\rangle$ and $\langle a(t)a(s)\rangle$ in the n- and a-spaces exhibits a more complicated dependence

$$\begin{aligned}\langle a(t)a(s)\rangle &= \int_{a,a'} a\, a' f(a,t;a',s)\mathrm{d}a\mathrm{d}a' \\ &= \int_{a,a'} a\, a' f(a,t|a',s)f(a',s)\mathrm{d}a\mathrm{d}a' \\ &= \int_{a'} a' \langle a|(a',s)\rangle f(a',s)\mathrm{d}a'.\end{aligned} \tag{8.1}$$

Making use of (7.5), we deduce

$$\begin{aligned}\langle a(t)a(s)\rangle &= \int_{a'} a' \sum_{n'} \langle n|(n',s)\rangle \frac{e^{-a'}a'^{n'}}{n'!} f(a',s)\mathrm{d}a', \\ &= \sum_{n'} \langle n|(n',s)\rangle \int_{a'} \frac{e^{-a'}a'^{n'+1}}{n'!} f(a',s)\mathrm{d}a'.\end{aligned} \tag{8.2}$$

Note that we have

$$\frac{e^{-a'}a'^{n'+1}}{n'!} = \left(-a'\frac{\partial}{\partial a'} + n'\right)\frac{e^{-a'}a'^{n'}}{n'!},$$

from which we deduce that

$$\begin{aligned}\int_{a'} \frac{e^{-a'}a'^{n'+1}}{n'!} f(a',s)\mathrm{d}a' &= \int_{a'} \left(-a'\frac{\partial}{\partial a'} + n'\right)\frac{e^{-a'}a'^{n'}}{n'!} f(a',s)\mathrm{d}a', \\ &= \int_{a'} \left(-a'\frac{\partial}{\partial a'} + n'\right)\frac{e^{-a'}a'^{n'}}{n'!} f(a',s)\mathrm{d}a, \\ &= n'P(n',s) - \int_{a'} \left(a'\frac{\partial}{\partial a'}\right)\frac{e^{-a'}a'^{n'}}{n'!} f(a',s)\mathrm{d}a.\end{aligned} \tag{8.3}$$

Since we have $\langle n(t)n(s)\rangle = \sum_{n'} n'P(n',s)\langle n|(n',s)\rangle$ and $\langle n|(a',s)\rangle = \langle a|(a',s)\rangle$, substituting (8.3) into (8.2) and making use of (7.4) leads to

$$\begin{aligned}\langle a(t)a(s)\rangle &= \langle n(t)n(s)\rangle - \sum_{n'}\int_{a'} \langle n|(n',s)\rangle \left(a'\frac{\partial}{\partial a'}\right)\frac{e^{-a'}a'^{n'}}{n'!} f(a',s)\mathrm{d}a, \\ &= \langle n(t)n(s)\rangle - \int_{a'} \left(a'\frac{\partial}{\partial a'}\right)\sum_{n'}\langle n|(n',s)\rangle\frac{e^{-a'}a'^{n'}}{n'!} f(a',s)\mathrm{d}a, \\ &= \langle n(t)n(s)\rangle - \int_{a'} \left(a'\frac{\partial}{\partial a'}\right)\sum_{n'}\langle n|(n',s)\rangle P(n',s|a',s) f(a',s)\mathrm{d}a, \\ &= \langle n(t)n(s)\rangle - \int_{a'} \left(a'\frac{\partial}{\partial a'}\right)\langle n|(a',s))\rangle f(a',s)\mathrm{d}a, \\ &= \langle n(t)n(s)\rangle - \int_{a'} \left(a'\frac{\partial}{\partial a'}\right)\langle a|(a',s))\rangle f(a',s)\mathrm{d}a, \\ &= \langle n(t)n(s)\rangle - \left\langle a'\frac{\partial}{\partial a'}\langle a|(a',s))\rangle\right\rangle.\end{aligned} \tag{8.4}$$

The final relation reads

$$\langle n(t)n(s)\rangle = \langle a(t)a(s)\rangle + \left\langle a'\frac{\partial}{\partial a'}\langle a|(a',s))\rangle\right\rangle. \tag{8.5}$$

Note that if we assume that t is sufficiently large for the conditional probability $f(a,t|a',s)$ to approach the steady state distribution $f_{ss} = \mathrm{Ga}(a;\alpha,\beta)$, then the second term on the right-hand side cancels out.

9. Fourier transforms

9.1. *Spread from a concentrated instantaneous source*

Using Fourier transform in the space variable, we can transform (4.7) of the paper

$$\frac{\partial \mathcal{F}}{\partial t} = -\frac{\mathcal{F}}{\mathrm{Pe}}\left(\omega^2 + \imath\omega\mathrm{Pe} + \mathrm{R}^2\right) \text{ with } \mathcal{F}(\omega,t) = \int_{-\infty}^{\infty} \tilde{\gamma}^*(\tilde{x},t)\mathrm{e}^{-\imath\omega\tilde{x}}\mathrm{d}\tilde{x}. \tag{9.1}$$

Given the initial condition:

$$\mathcal{F}(\omega,0) = \tilde{\Gamma}_0 \tag{9.2}$$

we can solve (9.1)

$$\mathcal{F}(\omega, t) = \tilde{\Gamma}_0 \exp\left[-\mathrm{Pe}^{-1}\left(\omega^2 + \imath\omega\mathrm{Pe} + \mathrm{R}^2\right) t\right] \tag{9.3}$$

Taking the inverse fourier transform of (9.3), we obtain:

$$\langle\tilde{\gamma}^*\rangle = \frac{\tilde{\Gamma}_0\sqrt{\mathrm{Pe}}}{\sqrt{4\pi\tilde{t}}} \exp\left[-\mathrm{Pe}\left(\frac{\left(\tilde{x}-\tilde{t}\right)^2}{4\tilde{t}} + \left(\frac{\mathrm{R}}{\mathrm{Pe}}\right)^2 \tilde{t}\right)\right]. \tag{9.4}$$

9.2. *Spatial correction and spectrum*

Using Fourier transform in the space variable, we can transform (4.20) of the paper in the limit $t \to \infty$

$$-\omega^2 D_u \mathcal{F} - \kappa\mathcal{F} + \mu\langle b\rangle_s = 0 \text{ with } \mathcal{F}(\omega) = \int_{-\infty}^{\infty} g_s(r)\mathrm{e}^{-\imath\omega r}\mathrm{d}\tilde{x}, \tag{9.5}$$

whose solution is straightforward

$$\mathcal{F} = \frac{\mu\langle b\rangle_s}{D_u\omega^2 + \kappa}. \tag{9.6}$$

Taking the inverse Fourier transform, we find

$$g_s(r) = \frac{1}{2}\frac{\mu\langle b\rangle_s}{\kappa\ell_c}\mathrm{e}^{-r/\ell_c} \text{ with } \ell_c = \sqrt{\frac{D_u}{\kappa}}. \tag{9.7}$$

FIGURE 5. Snapshot showing the tracking of the particles

10. Experiments 1: velocity probability distribution

We conducted experiments on a 2.5 meter long steep slope flume. The erodible bed was made of uni-sized natural sediment particles of mean diameter 8±1.5 mm. The flume was 8 cm wide and the water depth ranged from 1 to 3 cm during experiments. This setup was able to reproduce the fully turbulent flow of natural steep rivers, while avoiding complex 3-dimensional patterns like meanders and bars owing to the high water depth to channel width ratio. Moreover, the extremely narrow grain size distribution limited fluctuations due to size segregation and other related phenomena (Frey & Church 2009). Water discharge was adapted to meet the incipient motion condition (low Shields stress). Constant feeding of sediment guaranteed global equilibrium between erosion and deposition.

Particle motion was tracked using a high speed camera over a 40-cm length (Phantom v640 operated at 150 Hz with a field of 800×104 px). Trajectories of individual particles were captured using a particle tracking method based on the Matlab 'polyparticletracker' routines (Rogers *et al.* 2007). In addition to the particle tracking, sediment fluxes were measured both at the entrance and at the output of the flume by a new technique detailed as follows. Upon leaving the channel, each particle hits a metallic plate and the impact is recorded by a small accelerometer tied to the plate. A peak-over-threshold method is then applied to detect the times of the consecutive particle impacts. To validate the method, we measured the output weight of sediment systematically during experiments. See (Heyman *et al.* 2013) for further information.

Figure 5 shows a snapshot with the trajectories determined using the polyparticletracker-based Matlab script. Note that the bed was not free of bedforms and so the statistics of particle velocities was, to some degree, affected by these bedforms. As when conducting experiments over long times at low sediment transport stages, one is usually faced with such bed topography, we failed to obtain perfectly homogeneous bed configurations.

Figure 6 shows the same information as that presented in figure 8 in the paper, but in different ways. For the sake of comparison, figure 6(a) is the same as figure 8 in this paper. Looking at the cumulative distribution function shows that the truncated Gaussian function fits well the experimental data, the exponential distribution does not. The PP and QQ tests confirm this result. The QQ plot of figure 6(c) reveals, however, that there is a slight discrepancy between the truncated Gaussian function (3.41) of the paper and the empirical quantiles, but this could be anticipated as the particles can hardly move faster than the mean water flow.

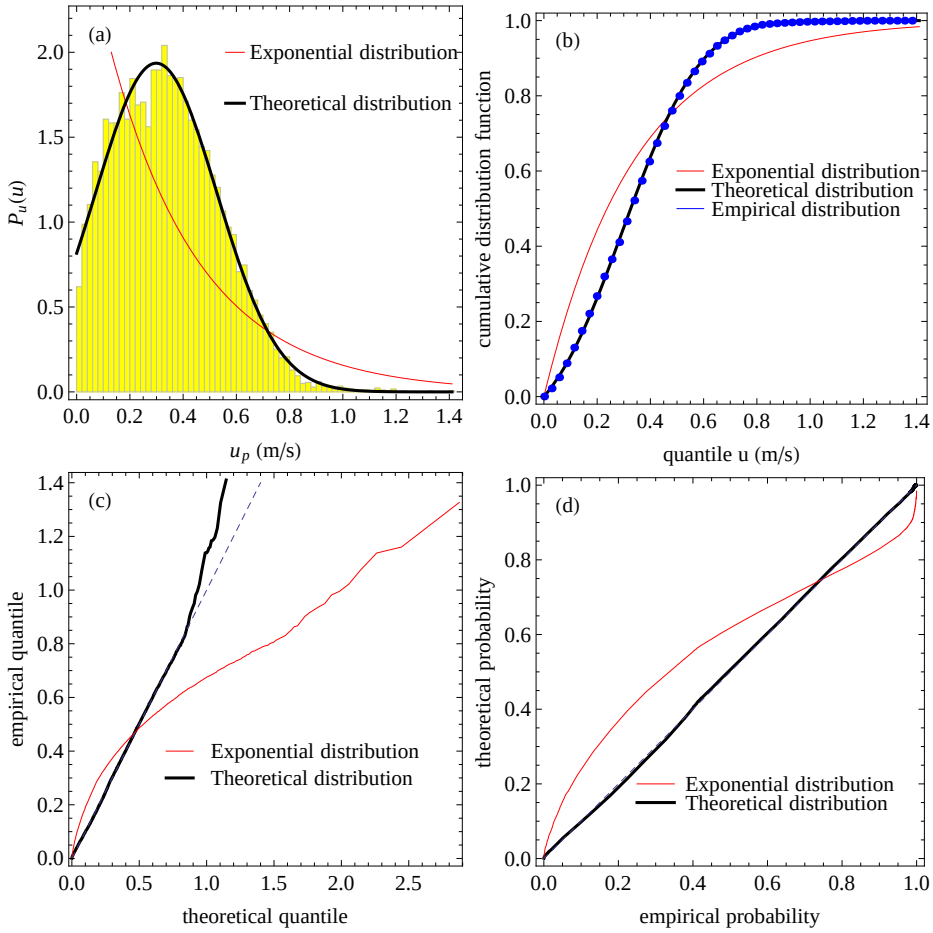

FIGURE 6. (a) Empirical probability density function (histogram) of the instantaneous particle velocities computed from 755 trajectories; the thick solid line is the theoretical distribution (3.41) of the paper, and for the sake of comparison, we have also plotted the exponential distribution (thin red curve). (b) Cumulative distribution function of the data and theoretical predictions. (c) QQ plot: we have plotted the empirical quantile as a function of the theoretical quantile. Perfect matching is achieved when the points collapse onto the first bissectrice. (d) PP plot: we have plotted the theoretical probability as a function of the theoretical probability. Perfect matching is achieved when the points collapse onto the first bissectrice. The flow conditions were the following: depth-averaged velocity of water $\bar{v} = 92.5$ cm s^{-1}, mean flow depth $h = 2$ cm, Froude number $\mathrm{Fr} = \bar{v}/\sqrt{gh} = 2.1$, flow Reynolds number $\mathrm{Re} = \bar{v}h/\nu_w = 18 \times 10^3$ (ν_w kinematic viscosity), Shields number $\mathrm{Sh} = \varrho h \sin\theta/[(\varrho_p - \varrho)d] = 0.042$.

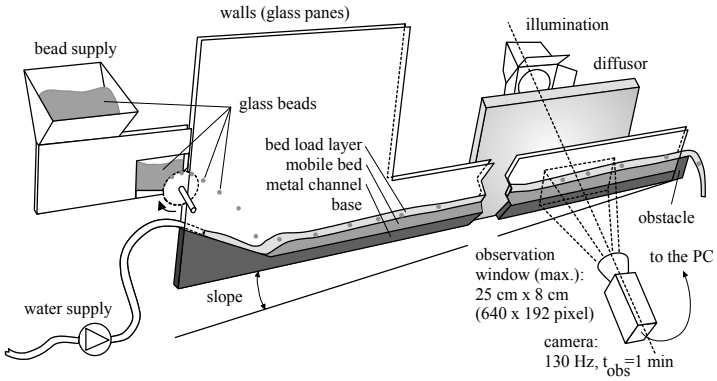

FIGURE 7. Sketch of the experimental setup.

11. Experiments 2: probability distribution of the particle transport rate for a fixed bed

11.1. *Experimental setup*

We conducted our experiments in a narrow flume in which sediment consisted of glass beads of equal size. This is very simple laboratory representation of bed load transport, with the advantages that boundary conditions are perfectly controlled and a wealth of information can be obtained using imaging techniques. Figure 7 sketches the experimental facility. The nearly two-dimensional feature of this facility has some disadvantages: for instance, the low width-to-depth ratio leads to hydraulic difficulties since turbulence may be controlled by the side walls rather than the bottom; and using spherical particles of the same size can be problematic in terms of bed arrangement, thus producing artificial conditions for particle entrainment. This is, however, the price paid for convenient access to the detailed flows.

Experiments were performed in a tilted, narrow, glass-sided channel, 2 m in length and 20 cm in height. The channel width B was adjusted to 6.5 mm, which was slightly larger than the particle diameter d. In this way, particle motion was approximately two-dimensional and stayed in the focal plane of the camera. The channel slope $\tan\theta$ ranged from 5% to 15%, but only experiments within the slope range 10% are reported here.

Coloured spherical glass beads with a nominal diameter of $d = 6$ mm and a density $\rho_p = 2500$ kg/m^3 (provided by Sigmund Lindner GmbH, Germany) were injected from a reservoir into the channel using a wheel driven by a direct current motor and equipped with 20 hollows on the circumference, as depicted in figure 7. For the experiments presented here, the injection rate $\dot{n}_0$ was 8.2 beads per second, with an uncertainty of less than 5%. The water supply at the channel entrance was controlled by an electromagnetic flow meter provided by Krohne (France). The discharge per unit width q_w was $5.39 \times 10^{-3}\,\mathrm{m}^2/\mathrm{s}$.

The hydraulic conditions (velocity profile, bed friction, etc.) have been described in earlier papers (Ancey *et al.* 2002; Böhm *et al.* 2004). Although the flume was narrow, its hydraulic characteristics were like those observed in wide channels with shallow flows (Frey & Reboud 2001).

The particles and the water stream were filmed using a Pulnix partial scan video camera (progressive scan TM-6705AN), placed perpendicular to the glass panes at 115 cm away from the channel, approximately 80 cm upstream from the channel outlet. The camera was inclined at the same angle as the channel, behind which lights were positioned. An

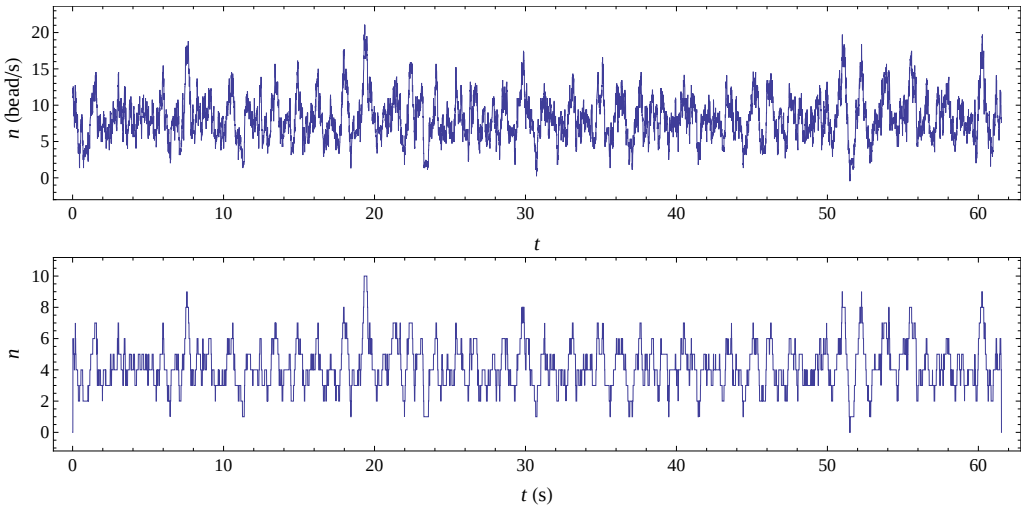

FIGURE 8. Times series of the number of moving particles and particle transport rate.

area of $\Delta x = 22.5$ cm in length and 8 cm in height was filmed and later reduced to accelerate image processing.

The camera resolution was 640×192 pixels for a frame rate of 129.2 fps (exposure time: 0.2 ms, 256 gray levels). Each sequence comprised 8000 images due to limited computer memory; this corresponded to a duration of approximately one minute. Images were analyzed using the WIMA software, provided by the *Traitement du Signal et Instrumentation* laboratory in Saint-Étienne (France). Positions of the bead mass centers were detected by means of an algorithm combining several image-processing operations; particle trajectories were calculated using a tracking algorithm (Böhm *et al.* 2006).

11.2. *Raw data*

figure 8 shows the times series of N and $\dot{n}$ used for the statistical treatment. The particle velocity varied within a wide range: the average value $\bar{u}_s$ and the standard derivation were 0.44 m/ s and 0.10 m/ s, respectively. The number of particles in the window (see Fig. 9) ranged from 0 to 10, with $\operatorname{var} N = 2.1$ and $\langle N \rangle = 4.2$.

11.3. *Analysis*

Figure 6 shows the same information as that presented in figure 9 in the paper, but in different ways. For the sake of comparison, figure 9(a) is the same as figure 9 in this paper. Looking at the cumulative distribution function shows that the theoretical distribution (3.45) does not perform well. The PP and QQ tests confirm this result.

The reason for this discrepancy is likely to be due to the non-Poissonian nature of the distribution of the number of moving particles, as shown by figure figure 10. This was probably the consequence of the supply system (consisting of a star wheel injecting particles at constant rate) and the short length of the flume (2 m), which made the arrival of particles more steady than wished.

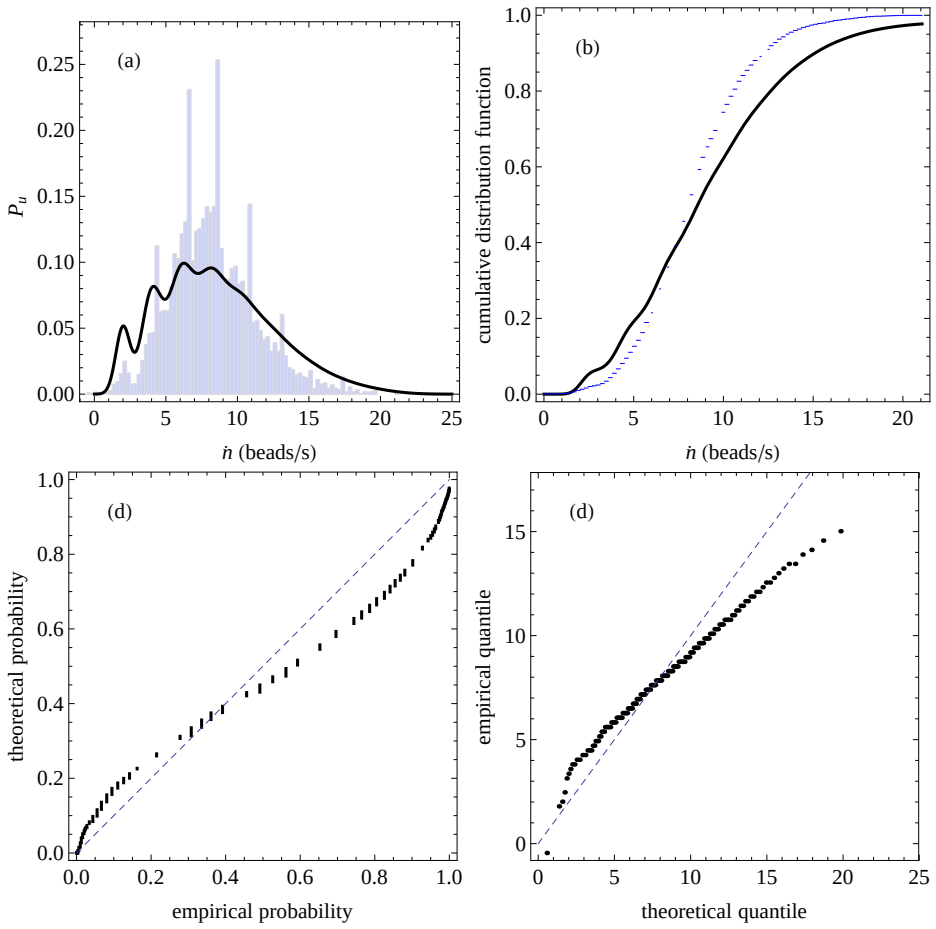

FIGURE 9. (a) Empirical probability density function (histogram) of the instantaneous particle flux computed from 8000 frames; the thick solid line is the theoretical distribution (3.45) of the paper. (b) Cumulative distribution function of the data and theoretical predictions. (c) QQ plot: we have plotted the empirical quantile as a function of the theoretical quantile. Perfect matching is achieved when the points collapse onto the first bissectrice. (d) PP plot: we have plotted the theoretical probability as a function of the theoretical probability. Perfect matching is achieved when the points collapse onto the first bissectrice. The flow conditions were the following: depth-averaged velocity of water $\bar{v} = 53$ cm s^{-1}, mean flow depth $h = 1$ cm, Froude number Fr $= 1.7$, flow Reynolds number Re $= 5300$, Shields number Sh $= 0.11$.

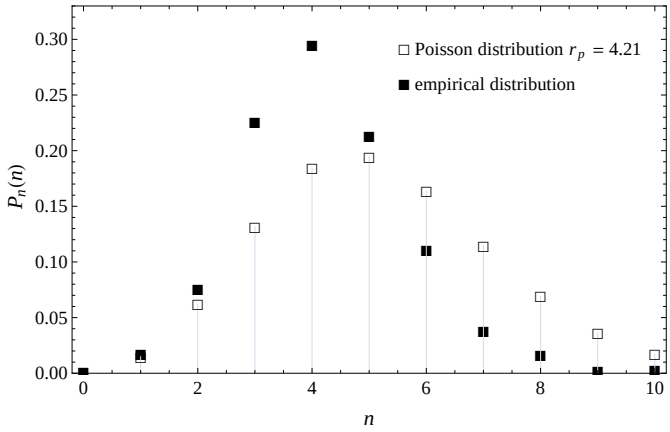

FIGURE 10. Empirical distribution function of the number of moving particle and comparison with a Poisson distribution.

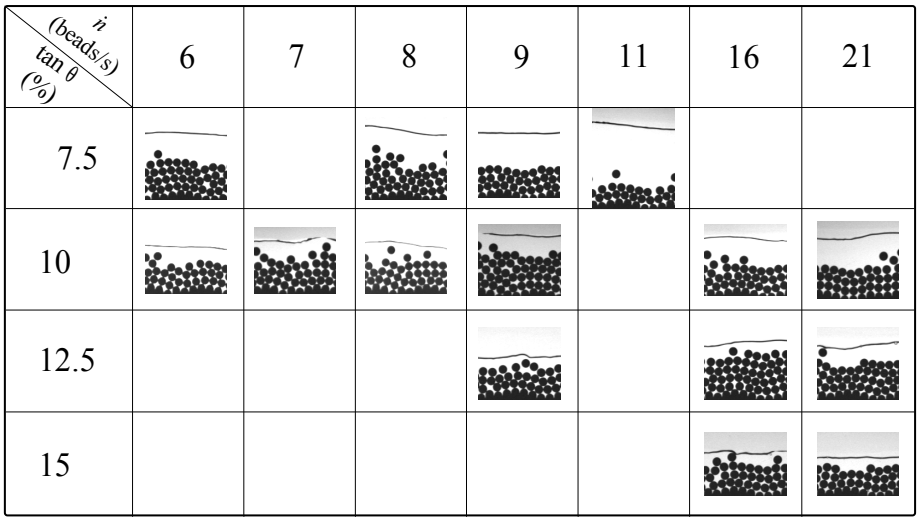

FIGURE 11. Overview of the experiments conducted at various solid discharges $\dot{n}$ and slopes $\tan\theta$. For each experiment, a detail of one filmed image is shown. See Tables 3 for the experimental conditions.

12. Experiments 3: probability distribution of the particle transport rate for a mobile bed

12.1. *Overview*

The experimental setup and data are presented in (Ancey *et al.* 2006) and (Ancey *et al.* 2008). The flume configuration is identical to that presented in § 9 except that now there is a bed composed of the same beads as those injected at the flume inlet. The channel base consisted of half-cylinders of equal size (radius $r = 3$ mm) and randomly arranged on different levels. Disorder was essential, as it prevented slipping of entire layers of particles on the upper bed surface, which would have induced artificial erosion conditions. The effects of bed disorder were addressed by Böhm *et al.* (2004).

We ran 15 experiments with different inclinations and various flow rates. Bed load equilibrium flows were achieved, as neither erosion nor deposition of particles occurred, averaged over sufficiently long time intervals. Table 3 summarizes the features of the 15 experiments. Figure 11 provides a snapshot of all of the experiments presented in this document.

12.2. *Results*

Figure 12 shows the empirical probability density function $P_n(n)$ and the theoretical distribution, which is the negative binomial law (3.17) in the paper. There is remarkably good agreement between data and theory for all experiments (see also the electronic supplement). Compared to our earlier findings (Ancey *et al.* 2008), this result shows that we can get rid of the emigration/immigration process (which was our first attempt to model the advection and dispersal of a particle current) without altering the performance of the model. As we investigated steady uniform flow conditions, this similarity of behaviour between the two formulations is not really a surprise. Further experimental work is under way to test the model under time-dependent non-uniform flow conditions.

Figure 13 shows the empirical and theoretical probability density functions $P_{\dot{n}}(\dot{n})$. In that case, concordance between theory and experiments is less marked for the experiments presented here; in the electronic supplement, we show that much better agreement is

Run	(a)	(b)	(c)	(d)	(e)	(f)	(g)	(h)	(i)	(j)	(k)	(l)	(m)	(n)	(o)
$\tan\theta$	0.07	0.07	0.07	0.07	0.10	0.10	0.10	0.10	0.10	0.10	0.12	0.12	0.12	0.15	0.15
$\dot{n}_0$	5.70	7.75	8.70	10.9	5.30	6.70	8.00	10.0	15.4	2.00	9.26	15.1	20.0	15.6	21.5
h	18.6	20.0	24.4	40.0	10.2	10.6	12.2	12.3	16.6	19.1	6.90	8.10	9.20	4.80	6.60
$\bar{v}$	53.7	57.7	56.7	65.3	40.8	41.7	44.3	45.1	49.3	54.1	43.0	47.6	48.6	48.0	44.6
$\mathrm{Re}\times 10^3$	10.0	11.5	13.8	26.2	4.20	4.40	5.40	5.50	8.20	10.3	3.00	3.80	4.50	2.30	2.90
Fr	1.26	1.30	1.16	1.04	1.29	1.29	1.28	1.30	1.22	1.25	1.65	1.69	1.62	2.21	1.76
Sh	0.14	0.15	0.19	0.30	0.10	0.11	0.12	0.12	0.17	0.19	0.09	0.10	0.12	0.07	0.10
$\bar{u}_{rol}$	0.08	0.08	0.08	0.08	0.06	0.07	0.06	0.07	0.07	0.07	0.07	0.07	0.08	0.07	0.08
$\bar{u}_{sal}$	0.35	0.36	0.33	0.30	0.28	0.29	0.29	0.28	0.31	0.31	0.23	0.27	0.30	0.18	0.22
$\bar{u}_s$	0.17	0.18	0.17	0.17	0.14	0.16	0.13	0.15	0.15	0.14	0.10	0.11	0.12	0.08	0.10
E	33.0	52.0	61.5	73.0	48.5	47.9	68.1	64.7	103	150	106	155	174	182	187
D	33.3	51.7	61.8	72.4	47.9	48.5	67.9	65.0	103	151	106	155	173	182	187
$\langle N\rangle$	7.10	9.80	12.2	14.9	9.50	9.90	13.8	13.7	22.8	34.2	21.9	32.4	38.5	43.3	47.9
$\mathrm{var}\, N$	22.5	30.9	35.4	38.5	70.7	36.8	64.5	49.1	72.0	128	123	182	222	214	130
$\langle\dot{n}\rangle$	5.45	7.76	9.20	10.9	5.72	6.85	7.74	9.41	15.5	20.5	9.52	15.5	19.8	15.4	20.5
σ	4.67	5.28	5.05	4.91	5.13	4.86	4.95	4.74	4.52	4.39	4.84	4.77	4.51	4.21	3.90
μ	3.21	3.61	3.31	3.01	4.44	3.56	3.89	3.42	3.09	3.23	3.94	3.93	3.73	3.36	2.47
λ'	10.3	16.5	21.1	28.1	6.48	12.8	14.5	18	32.7	39.89	18.7	27.4	30.0	36.8	68.7

TABLE 3. Flow characteristics for experiments (e), (g), (i), and (j) carried out. Varying parameters: flume slope $\tan\theta$ and inflow rate $\dot{n}_0$ (beads s^{-1}). Water flow characteristics $\bar{v}$ ($\mathrm{m\,s}^{-1}$) and h (mm) and time-averaged values of the Reynolds, Froude, and Shields numbers characterizing bed load and water flow. For each experiments, we measured the particle velocity $\bar{u}_{rol}$ ($\mathrm{m\,s}^{-1}$) in the rolling regime, their velocity $\bar{u}_{sal}$ ($\mathrm{m\,s}^{-1}$) in the saltating regime, the mean particle velocity $\bar{u}_s$ ($\mathrm{m\,s}^{-1}$). We also measured the mean number of deposited/entrained particles and then deduced the entrainment and deposition rates E (beads s^{-1}) and D (beads s^{-1}). We also counted the mean number of moving particles$\langle N\rangle$ as well as its variance $\mathrm{var}\, N$. We deduced the mean particle flux $\langle\dot{n}\rangle$ (beads s^{-1}) in the control volume. From the deposition and entrainment rates together with the number of moving particles, we inferred estimates of the entrainment and deposition parameters μ (s^{-1}), λ' (s^{-1}) and σ (s^{-1}). See the electronic supplement for the whole set of experiments.

obtained at steeper slopes. One possible reason for this discrepancy is the existence of two populations of moving particles with two distinctive mean velocities. As shown by table 3, there is a factor of about 5 between the velocities in the rolling and saltating regimes. Comparing the different runs also shows that the larger the number of moving particles, the better the agreement. This may be an indication that either theory performs less in the limit $N \to 0$ or the computation of the sediment transport rate is biased as we did assume that the the probabilities $P_n(n)$ and $P_u(u_p)$ were independent such that we could obtain $P_{\dot{n}}(\dot{n})$ by taking the Fourier transform of the convolution product. This is point that still requires further work.

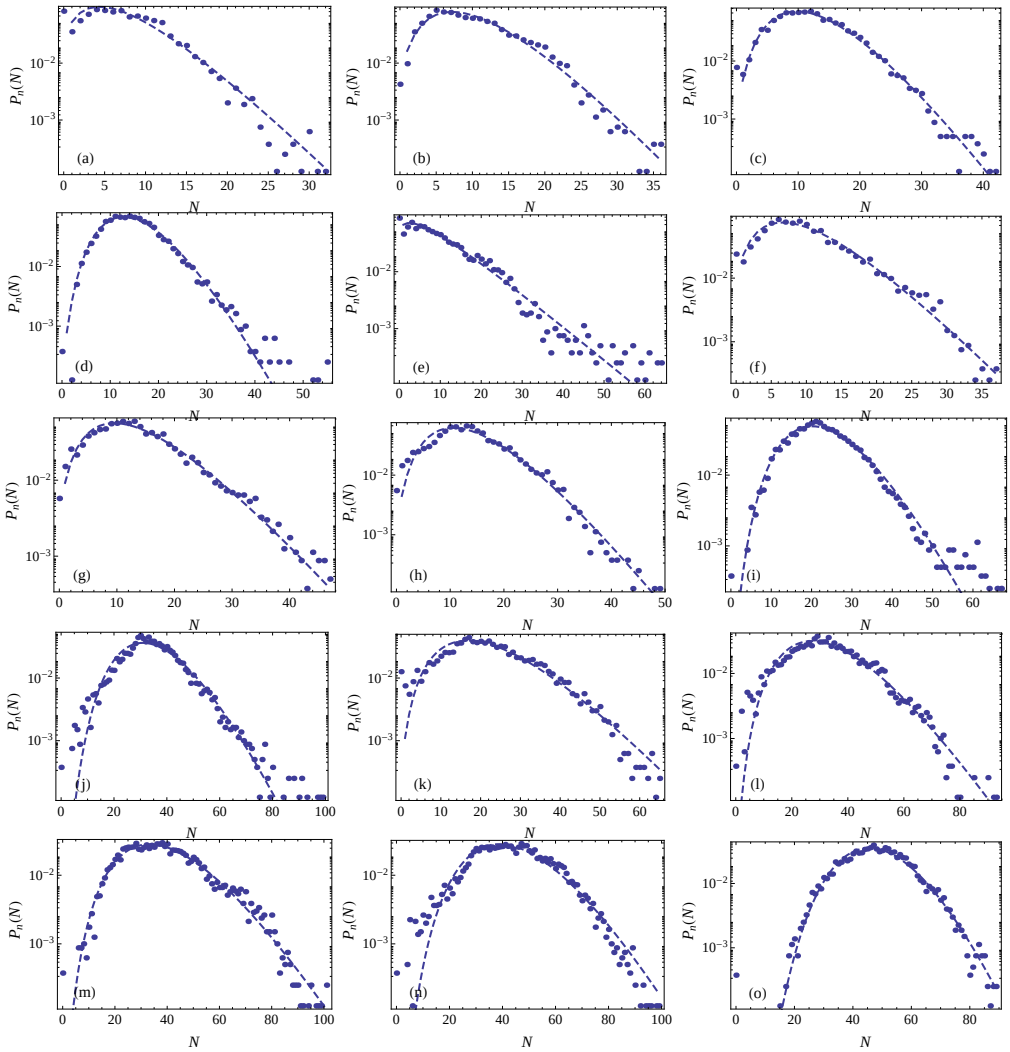

FIGURE 12. Probability density function for the number of moving particles in experiments (a) to (o). The dots represent the empirical probability density while the dashed curves are the theoretical distributions (3.17) of the paper.

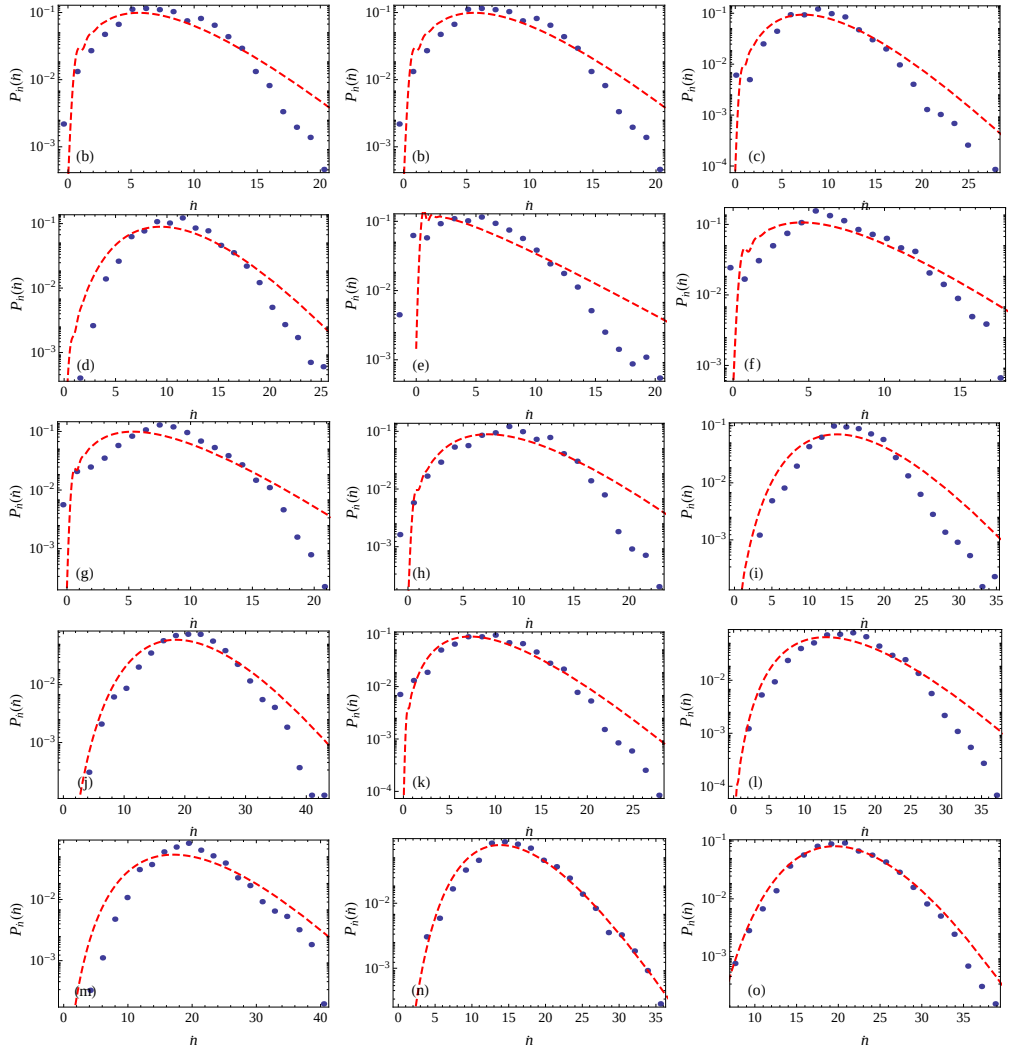

FIGURE 13. Probability density function for the particle flux in experiments (a) to (o). The dots represent the empirical probability density while the dashed curves are the theoretical distributions (3.45) with $\zeta = 4$. This parameter was fixed arbitrarily, but provided that $\zeta > 3$, we found that altering ζ did not change the shape of $P_{\dot{n}}(\dot{n})$ significantly for these runs

REFERENCES

Ancey, C., Bigillon, F., Frey, P., Lanier, J. & Ducret, R. 2002 Saltating motion of a bead in a rapid water stream. *Phys. Rev. E* **66**, 036306.

Ancey, C., Böhm, T., Jodeau, M. & Frey, P. 2006 Statistical description of sediment transport experiments. *Phys. Rev. E* **74**, 011302.

Ancey, C., Davison, A. C., Böhm, T., Jodeau, M. & Frey, P. 2008 Entrainment and motion of coarse particles in a shallow water stream down a steep slope. *J. Fluid Mech.* **595**, 83–114.

Böhm, T., Ancey, C., Frey, P., Reboud, J.-L. & Duccotet, C. 2004 Fluctuations of the solid discharge of gravity-driven particle flows in a turbulent stream. *Phys. Rev. E* **69**, 061307.

Böhm, T., Frey, P., Duccotet, C., Ancey, C., Jodeau, M. & Reboud, J.-L. 2006 Two-dimensional motion of a set of particles in a free surface flow with image processing. *Exper. Fluids* **41**, 1–11.

Cox, J.C., Ingersoll, J.E. & Ross, S.A. 1985 A theory of the term structure of interest rates. *Econometrica* **53**, 385–407.

Feller, W. 1951 Two singular diffusion problems. *Ann. Math.* **54**, 173–182.

Frey, P. & Church, M. 2009 How River Beds Move. *Science* **325**, 1509–1510.

Frey, P. & Reboud, J.-L. 2001 Experimental study of narrow free-surface turbulent flows on steep slopes. In *Advances in flow modeling and turbulence measurements* (ed. H. Ninokata, A. Wada & N. Tanaka). Singapore: World Scientific Publishing.

Furbish, D.J., Haff, P.K., Roseberry, J.C. & Schmeeckle, M.W. 2012 A probabilistic description of the bed load sediment flux: 1. Theory. *J. Geophys. Res.* **117**, F03031.

Gardiner, C.W. 1983 *Handbook of Stochastic Methods*. Berlin: Springer Verlag.

Heyman, J., Mettra, F., Ma, H.B. & Ancey, C. 2013 Statistics of bedload transport over steep slopes: Separation of time scales and collective motion. *Geophys. Res. Lett.* **40**, 128–133.

Pedersen, A.R. 2000 Estimating the nitrous oxide emission rate from the soil surface by means of a diffusion model. *Scandinavian Journal of Statistics* **27**, 385–403.

Rogers, S. S., Waigh, T. A., Zhao, X. & Lu, J. R. 2007 Precise particle tracking against a complicated background: polynomial fitting with Gaussian weight. *Phys. Biol.* **4**, 220–227.

Sacerdote, L. 1990 On the solution of the Fokker-Planck equation for a Feller process. *Adv. Appl. Prob.* **22**, 101–110.